Quantized Collision/Fusion Events of Anionic Ionosomes at a Polarized Soft Micro-interface

Jingcheng Zhang,[a] Linhan Huang, [a] Zhipeng Xiang,*[b] Pekka Peljo,[c] Shiyu Gan,[d] Xinjian Huang,[e] and Haiqiang Deng*[a]

[a] J. Zhang, L. Huang, Prof. Dr. H. Deng
School of Chemical Engineering and Technology
Sun Yat-sen University
Zhuhai 519082, China

E-mail: denghq9@mail.sysu.edu.cn

[b] Dr. Z. Xiang
Guangdong Provincial Key Laboratory of Fuel Cell Technology, School of Chemistry and Chemical Engineering
South China University of Technology
Guangzhou 510641, China

E-mail: xzp20209094@scut.edu.cn

[c] Prof. Dr. P. Peljo
Research Group of Battery Materials and Technologies, Department of Mechanical and Materials Engineering, Faculty of Technology
University of Turku
20014 Turun Yliopisto, Finland

[d] Prof. Dr. S. Gan
Guangzhou Key Laboratory of Sensing Materials & Devices, Center for Advanced Analytical Science, School of Chemistry and Chemical Engineering
Guangzhou University
Guangzhou 510006, China

[e] Dr. X. Huang
Institute of Intelligent Perception
Midea Corporate Research Center
Foshan 528311, China

Supporting information for this article is given via a link at the end of the document.

Abstract: Single-entity collisional electrochemistry (SECE) can capture physicochemical information at the single entity level. In the present work, we systematically studied in-situ generation and detection of single anionic ionosomes via SECE combined with a miniaturized interface between two immiscible electrolyte solutions (ITIES). Ionosome is an ionic-bilayer encapsulated nanoscopic water cluster/droplet that carries a net charge. Discrete spiky ionic currents were observed upon collisions/fusions of individual Cl^-–ionosomes with a positively polarized micro-ITIES. This fusion process was proved to follow the bulk electrolysis model. With this method, some essential effects such as the interfacial area, concentration and charge density of the hydrated anions were revealed.

It demonstrates that anionic ionosomes share a common theoretical framework with their counterparts (i.e., cationic ionosomes, like Li^+–ionosomes). This work will spur the advancements in a myriad of fields, including such as the colloid and interface science, micro- and/or nanoscale electrochemistry, and electrophysiology and brain sciences.

Introduction

Single-entity collisional electrochemistry (SECE) has emerged in the past two decades, in which many excellent works have been reported.[1] It can reveal the intrinsic structure–activity relationship of the electrocatalytically active particles,[2] shed new light on the particle-electrode interaction dynamics,[3] and hence effectively avoid the averaging ensemble effect originated from the conventional technologies. So far, a number of studies on both the "hard" (e.g., Ag, Au, TiO_2, polystyrene) particles and the "soft" (e.g., oil-in-water (o/w) or water-in-oil (w/o) emulsions, liposomes, DNA and proteins, and viruses) particles have been reported.[4] For the latter, much work has focused on the interactions between individual emulsion droplets and a detecting ultramicroelectrode (UME). For the o/w emulsions, a lipophilic redox-active species is confined within the dispersed phase, i.e., the emulsion oil droplets; once the oil droplets dispersed in an aqueous continuous phase collide with the UME polarized at a constantly appropriate (e.g., diffusion-controlled) potential, an electron transfer (ET) reaction between the redox species and the UME occurs. Ion transfer (IT) at the oil droplets/water (o/w) interface is coupled to ET to maintain the electroneutrality within the droplets. In the aforementioned Cottrell-type experiment, the resulted current (*i*) is recorded as a function of time (*t*). Typically, spiky *i*–*t* signals with discreteness for the SECE of emulsion droplets are observed. Note that most studies in this field employ chronoamperometry as the signal readout method,[5] even though fast-scan cyclic voltammetry[6] and Fourier-transformed sinusoidal voltammetry[7] have also been successfully introduced. The charge (i.e., enclosed area under a spike), *i*–*t* profile, frequency of the spikes can be used to extract pivotal information including the encapsulated contents/emulsion size distribution, kinetics of bulk electrolysis within individual emulsion droplets, and concentration of emulsion droplets, etc.[5]

Microscopic mechanism for the transport of ions across the interface between two immiscible electrolyte solutions (ITIES), which involves multiple elementary steps, like diffusion/migration, formation/breakage of a water finger, and ion pair formation, among others, are gradually revealed with the advances in both experiments and theory.[8] Based on these fundamental achievements, applications of IT reactions at the ITIES have encompassed such as hydrometallurgy,[9] chemical sensing,[10] phase transfer catalysis,[11] imaging over nanopores,[12] and even electrochemical attosyringe.[13] In 2017, Laborda et al. opened up a new avenue for investigation of electrochemical stochastic events at the polarized ITIES.[14] They filled the ionic probes (e.g., Cl^-, or tetramethylammonium cation) in the emulsion oil droplets that are dispersed in the water continuous phase, and the ionic current spikes were observed in the potentiostatic *i*–*t* trace when individual droplets collided/fused with the sub-millimeter 1,2-dichloroethane (DCE)/water (w) interface. The collisions/fusions of micro- (or nano-) scale emulsion droplets containing hydrophilic or hydrophobic ions with the polarized ITIES mimics the ion transfer processes at the cellular membrane in nature. While the ionic fluxes crossing cellular membrane underlies a number of fundamental biological processes, such as the electrical signaling in the nervous system.[15] Their work has been extended and deepened by several other groups including Samec,[16] Stockmann and Kanoufi,[17] and also ourselves,[18] etc.

In the previous work, we found that IT reaction can spontaneously form a subtype of w/o nano-/microemulsions (e.g., Li^+–ionosomes or Cl^-–ionosomes, viz. nanoscopic water clusters/droplets that are wrapped by an ionic bilayer). The generation and the ensuing detection of ionosomes at the single-entity level was achieved with a double–potential step chronoamperometry.[18a] Briefly, small

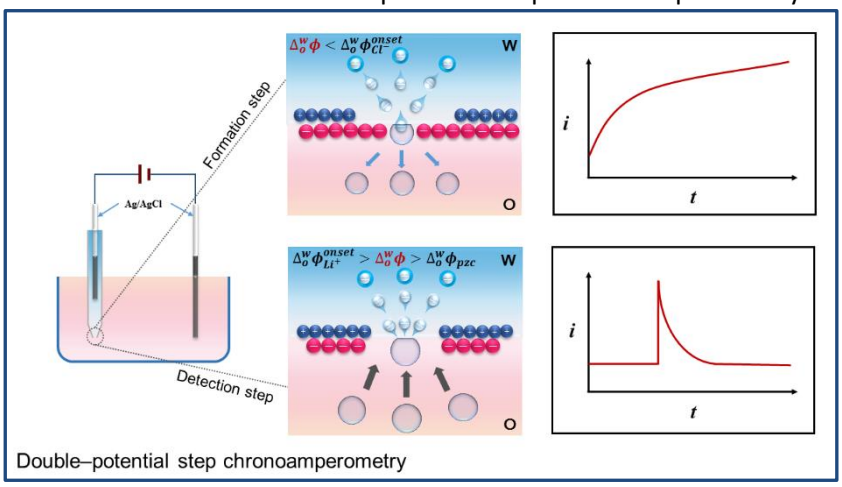

Figure 1. Schematic diagram (not to scale) of the discrete Cl^-–ionosomes collisions/fusions experiment at the micro-ITIES (left panel) formed at the tip of a micropipette. The micropipette contains an aqueous electrolyte solution of LiCl, and is immersed in the outer organic electrolyte solution. The middle panel is the general principle of electrochemical in-situ generation and detection of Cl^-–ionosomes, in which *pzc* denotes the potential of zero charge; and right panel represents the corresponding *i*–*t* responses. Note that the lipophilic counter-ion bis(triphenylphosphoranylidene)ammonium (BA^+) is coupled with the hydrated Cl^- in the organic phase, forming an ionic bilayer that wraps the ionosomes. The structure of ionosomes is not detailed herein.

hydrated cations (e.g., Li^+), are driven into an immiscible oil phase containing bulky supporting electrolyte by a sufficiently positive bias applied at the micro-ITIES. Lipophilic counter-anions (e.g., TB^-, abbreviated for tetrakis(pentafluorophenyl)borate anion) in the oil phase correlate electrostatically with the hydrated cations, generating a small amount of Li^+–ionosomes. Note that either Li^+–ionosomes or Cl^-–ionosomes bear a net positive or negative charge, respectively.[18a] This is caused by the steric limitation of very bulky lipophilic counter-ions facing with the inner hydrated cations that are hexagonally packed onto the water cores of the ionosomes. Once we reverse the bias at the micro-ITIES, these ionosomes collide/fuse with the negatively polarized (water vs. oil) micro-ITIES, accompanying destruction of their ionic bilayers and return of Li^+ into the water phase. This process is manifested as a train of ionic current spikes on a potentiostatic *i*–*t* trace. By analyzing these spikes, quantitative information including the size distribution and concentration of the ionosomes can be obtained. Besides discovery of the ionosomes, another highlight of this work is that the analytes – ionosomes do not need to be prepared in advance, effectively avoiding the issue of aggregation/agglomeration that is often encountered in the previous SECE stuides[14, 17a, 18b] The only exception is a generation/collection-like mode of electrocatalytic SECE enabled by scanning electrochemical microscopy.[19] This setup is certainly more complicated, compared with our developed double–potential step chronoamperometry for generation and in-situ detection of single ionosomes.

Herein, we continue to scrutinize the in-situ formation and detection of anionic Cl^-–ionosomes with this convenient double–potential step chronoamperometry. We introduce the bulk electrolysis model to study the *i*–*t* decay behavior of current spikes. It shows that fusion of an ionosome with the polarized micro-ITIES follows this model, similar to electrolysis of a single redox-active emulsion droplet at a solid UME/electrolyte interface. We also investigate some other factors, such as halogen anions with different charge densities, concentration of halogen anions, interfacial area of the ITIES,

along with the effect of tetrafluoroborate (BF_4^-) anion, to observe their influences on the formation of anionic ionosomes. It is found that both the halogen anions of higher charge density and the larger interfacial area of the ITIES contribute positively to the spontaneous formation of anionic ionosomes. However, when we increase the concentration of aqueous supporting electrolyte like LiCl, the formation of (e.g., Cl^-–) ionosomes via electrochemical polarization is inhibited. Adding BF_4^- which is easier transferrable anions within the polarizable potential window (PPW), helps to form more Cl^-–ionosomes. This is evidenced by the frequency of collision/fusion events from the pre-formed Cl^-–ionosomes under a constant cathodic bias at the micro-ITIES.

Results and Discussion

$$\mathrm{Ag}\,|\,\mathrm{AgCl}\,|\,\underset{\substack{x=10,100,1000\\(aq.\text{ in micropipette})}}{x\text{ mM LiCl}}\,\Big|\,\underset{(TFT)}{5\text{ mM BATB}}\,|\,\mathrm{AgCl}\,|\,\mathrm{Ag} \qquad \text{(cell 1)}$$

$$\mathrm{Ag}\,|\,\mathrm{AgCl}\,|\,\underset{\substack{Y=\mathrm{Cl,Br,I}\\(aq.\text{ in micropipette})}}{10\text{ mM Li}Y}\,\Big|\,\underset{(TFT)}{5\text{ mM BATB}}\,|\,\mathrm{AgCl}\,|\,\mathrm{Ag} \qquad \text{(cell 2)}$$

$$\mathrm{Ag}\,|\,\mathrm{AgCl}\,|\,\underset{(aq.\text{ in micropipette})}{\begin{matrix}10\text{ mM LiCl}\\+0.5\text{ mM }LiBF_4\end{matrix}}\,\Big|\,\underset{(TFT)}{5\text{ mM BATB}}\,|\,\mathrm{AgCl}\,|\,\mathrm{Ag} \qquad \text{(cell 3)}$$

Scheme 1. The electrochemical cell composition.

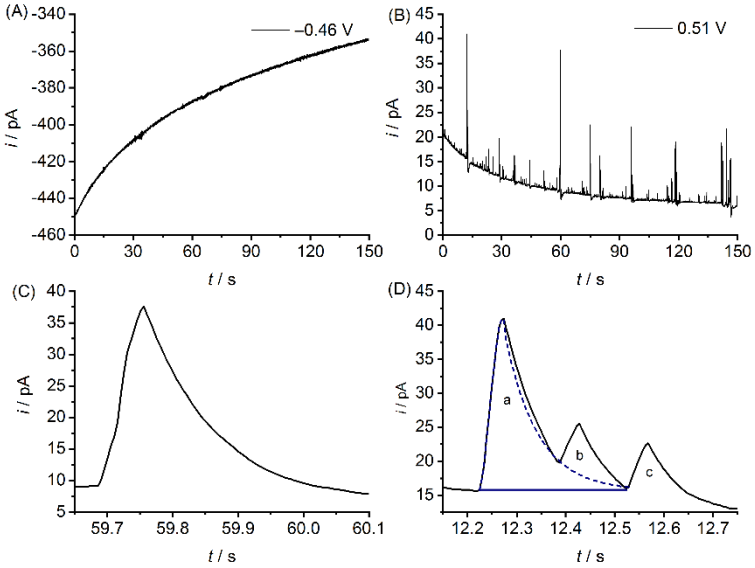

Figure 2. (A) Amperometric *i*–*t* curve recorded at the Galvanic potential of –0.46 V for the transfer reaction of Cl^- ions crossing the water/TFT ITIES (detailed in electrochemical cell 1, *x* = 10, Scheme 1) supported at the orifice of a 2.8 μm inner-diameter (i.d.) micropipette (Figure S2, SI). The sampling time is 5 ms among the data point. (B) The *i*–*t* curve recorded for the collisions and fusions of individual Cl^-–ionosomes with the water/TFT ITIES when we applied the constant +0.51 V to the same electrochemical cell I at the end of experiment conducted in panel "A". Note that the selection of the Galvani potentials is based on the cyclic voltammogram (CV) of cell I (Figure S1, SI), and the aforementioned two Galvani potentials can meet the requirements for generation and detection of Cl^-–ionosomes. (C and D) Zoom-in ranges of 59.65–60.10 s and 12.15–12.75 s of panel B, respectively. A spike is assumed to represents a collision and fusion event per ionosome. The successive collisions/fusions of ionosomes "a", "b", and "c" show partially overlapped multi-peak current signals in panel D (in which the blue solid and dashed lines represent the residency time and the current trajectory of a presumed full spike "a"). Note that the current spikes "b" and "c" are fully resolved and not overlapped.

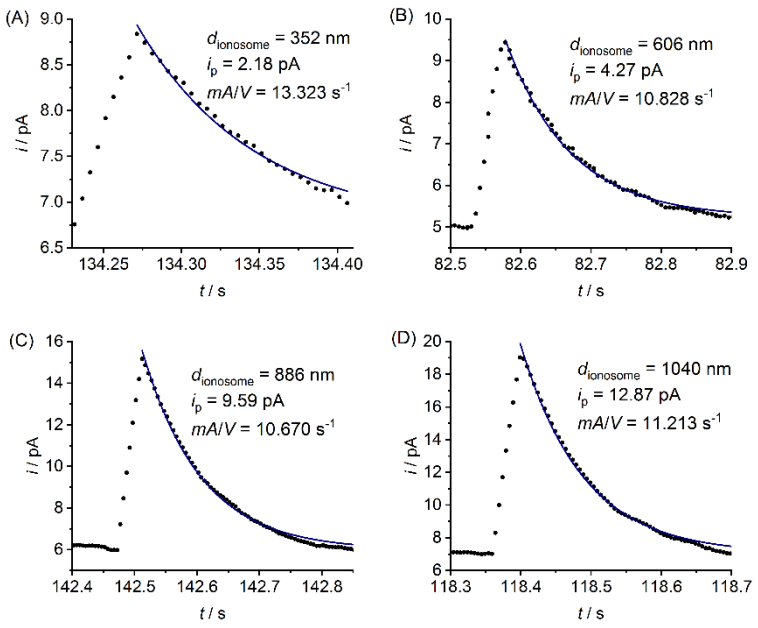

Figure 3. (A–D) Zoom–in and fitting of the experimental current spikes that are originated from Figure 2B. The experimental data were sampled every 5 ms (black dots). The simulated *i–t* decay trace (solid blue line) was obtained using eq. 2. The diameter of an ionosome, $d_{ionosome}$, is calculated from eq. 1, *i*p and the analogous first-order rate constant *mA/V* are extracted from the simulated curves.

Dection of Single Cl^-–ionosomes by Ion Transfer Reaction. The general principle of the electrochemical generation and ensuing in-situ detection of single ionosomes have been described in our previous work.[18a] The *i–t* curves in Figure 2 were obtained with the electrochemical cell 1 (*x* = 10) detailed in Scheme 1. When we applied a sufficiently negative Galvani potential viz. –0.46 V that exceeds the onset transfer potential of Cl^- (about –0.35 V, Figure S1 in the Supporting Information (SI)) for 150 s (Figure 2A), hydrated Cl^- ions enter the α,α,α-trifluorotoluene (TFT) phase and spontaneously form anionic ionosomes (denoted as Cl^-–ionosomes) at the TFT side of the water/TFT interface, as evidenced in Figure 2B. Specifically, reversing the polarization and maintaining+0.51 V at the water/TFT micro-ITIES, plenty of unidirectionally positive current spikes were observed along with a gradually decreasing background current, as shown in Figure 2B. The background current levels off for quite a long time, thus excluding the possibility of a more efficient (hemi-)spherical diffusion of small molecules/ions from the outer organic solution towards the micropipette orifice. Note that this phenomenon was often seen in our prior work[5c] and is more likely caused by the slower migration and/or diffusion of anionic Cl^-–ionosomes from the interior of TFT phase towards the TFT/water ITIES[5b]. These quantized spiky signals represent collisions/fusions of single anionic Cl^-–ionosomes with the polarized micro-ITIES one at a time, which manifests as a sharp current rise in a short time (i.e., kiss and burst) followed by a slowly decay in a longer time. Positive sign of the spikes suggests that hydrated Cl^- ions are released from each Cl^-–ionosome and then return back into the aqueous phase. Because stay of Cl^- ions in the TFT phase is thermodynamically unfavorable under this potential. This situation is very similar as the previous reports.[16a, 18b, 20] Then, we are noted that these signals can be simply divided into two types in the amperometric *i–t* traces: 1) single-peak spikes (i.e., singlets, 95%), 2) multi-peak spikes (i.e., multiplets, 5%), just as those shown in Figure 2C and D, respectively. There is no doubt that an individual collision and fusion event leads to a surge and the following slower decay of current, but the multi-peak current is a different scenario with respect to previous studies.[21] For example, Stockmann et al. reported catalytic activation of the heterogeneous oxygen reduction reaction by impact events between single Pt nanoparticles (NPs) and a polarized water/DCE micro-ITIES.[17a] The oxidation of the intermediate – ferrocene hydride

donates electrons to molecular oxygen facilitated via a bipolar Pt NP. Their result also shows multi-peak spikes with uniform intensity and residency time in the recorded *i*–*t* curve. They explained that the multiplet results from the same one larger-sized cluster of Pt NPs bouncing on the ITIES. However, such agglomeration unlikely occurs for our SECE measurements because the Cl^- −ionosomes bear a net negative charge, making unfavorable agglutination among them due to the electrostatic repulsion. This argument is also supported by the gradually decaying positive background current that commences at about 20 pA and then stabilizes at 5 pA in the range of 150 to 300 s (Figure S3, SI). The pattern of background current likely unveils this scenario: migration and/or diffusion towards the oil side of the ITIES of both the anionic Cl^-–ionosomes and the Cl^- ions that are not involved in assembling the Cl^-–ionosomes results in this ionic background current. The steady-state delivery of unreacted Cl^- ions dictates the stabilized background current. Note that this background current represents a Faradaic rather than a non-Faradaic process. Hence, it is understandable that this effect is more pronounced only when a sufficient number of anionic ionosomes are generated and then approach the micro-ITIES. In Figure 2D, we note that spikes "a" and "b" are partially overlapped. When Cl^- ions trapped by an ionosome "a" has not yet been exhausted during a single fusion event, another ionosome "b" collides the micro-ITIES and releases Cl^- ions simultaneously, dominating the current magnitude of a presumed full spike "a". While, in Figure 2D, the fusion events of "b" and "c" are fully resolved. By integrating the area of corresponding current signal vs. time, the charge released by three Cl^-–ionosomes are 1770, 390, and 490 fC, respectively. Afterwards, the radii of Cl^-–ionosomes can be calculated by eq. 1,

$$r_{ionosome} = \sqrt{\frac{QA_{\mathrm{Cl}^-}}{4\pi\eta_h e^-}} + d_{\mathrm{BA}^+} \qquad (1)$$

where A_{Cl^-} is the surface area of a spherical hydrated Cl^- anion,[22] Q is the charge of each Cl^- −ionosomes, η_h is the hexagonal packing density, e^- is the elementary charge, and d_{BA^+} is the diameter (≈1.3 nm) of bis(triphenylphosphoranylidene)ammonium cation (BA^+). The radii of the aforementioned three Cl^-–ionosomes are calculated to be 581, 273, and 306 nm, respectively. Therefore, for ionosomes with comparable radii, their charge plays an important role in the successive collision behaviors.

In terms of detecting the discrete collisional events, several key points are summarized as follows: 1) under detecting potentials that are more positive than the *pzc*, the polarized ITIES attracts both negatively-charged Cl^-–ionosomes and unreacted Cl^- ions, which manifests as a train of spikes superimposed onto a stable-after-an-initial-decay background current; 2) in general, the background current increases with the increase in the electrochemically generated ionosomes (under conditions of a larger bias and a longer time); 3) due to electrostatic repulsion between ionosomes with the like charge, they are hardly to aggregate/coalesce; and 4) multiplets result from successive collisions and fusions of adjacent ionosomes.

Next, we attempted to acquire some more insights about fusions of ionosomes by fitting the bulk electrolysis model with the experimental current spike.[23] Previous studies have shown that collisions/fusions of the ion-loaded single emulsion droplets with a polarized ITIES share a common

feature with the individual metal particle electrolysis on a metallic UME, where the current exponentially decays with time.[14, 24] However, the specific mechanisms of the two are quite different. Regarding the former, when an emulsion droplet collides with a polarized ITIES, it will fuse with the soft interface and open a small pore. This connects the droplet to the interface for sensing the propagation of the interfacial potential difference, and then the encapsulated ionic species strip from the emulsion droplet to another adjacent phase. Likewise, the bulk electrolysis model is also applicable to fusion of an ionosome with a polarized ITIES. The *i*–*t* behavior obeys the expressions shown below:

$$i(t) = i_{\mathrm{p}} e^{-(mA/V)t} \qquad (2)$$

$$m = \frac{4D_{\mathrm{Cl}^-}}{\pi r_{\mathrm{c}}} \qquad (3)$$

where i_{p} is the magnitude of a current spike, m is the mass-transfer coefficient of the Cl^-ions within the Cl^-–ionosome droplet, A is the area of the fusion pore connected to the aqueous phase and can be calculated from r_{c} (i.e., πr_{c}^2), r_{c} is the Cl^-–ionosome effective contact (i.e., the fusion pore) radius, V is the volume of a Cl^-–ionosomes, t is the time elapsed (in second), and D_{Cl^-} is the diffusion coefficient of Cl^- ions in water. Note that the volume of an ionosome, V, is calculated with the formula $(4/3)\pi r_{\mathrm{ionosome}}^3$, where r_{ionosome} is obtained by eq. 1.

Typically, the rising branch of a current spike peaks within 50 ms and then decays in the exponential manner to the baseline (see Figure 3, A–D). The experimental current spikes were fitted using the eq. 2. Clearly, the theoretical *i*–*t* traces (solid blue lines) agree well with the experimental *i*–*t* ones (black dots), implying that the ion transfer reaction from a Cl^-–ionosome into the aqueous side of a polarized ITIES also follows the bulk electrolysis model. The best-fitting theoretical curve can provide the analogous first-order rate constant, $k = mA/V$. Rearranging eqs. 2, 3, and that of V, yields

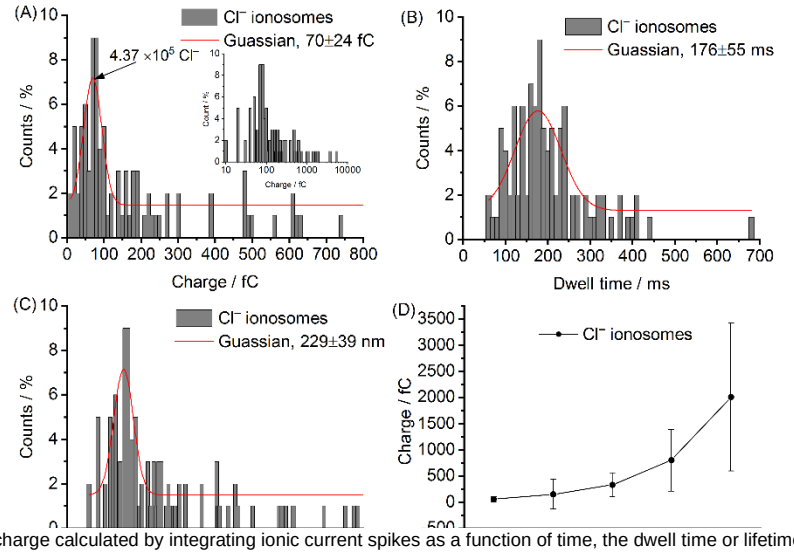

Figure 4. (A, B, and C) Statistical histograms of the charge calculated by integrating ionic current spikes as a function of time, the dwell time or lifetime of the ionic current spikes, and diameter of Cl^-– ionosomes. Calculation of the diameter of ionosomes is based on the assumption that smaller hydrated chloride anions pack on the surface of the larger water cores of ionosomes in the closest hexagonal grid. (D) The scatter plot for the relation between the dwell time and the corresponding charge of Cl^-– ionosomes. The plot produces bigger errors for the largest Cl^-–ionosomes because the population of Cl^-–ionosomes with a longer dwell time spanned between 400 and 500 ms is much smaller.

$$\frac{mA}{V} = \frac{3r_c D_{Cl^-}}{\pi r_{ionosome}^3} \quad (4)$$

Combining the best-fitting theoretical curve and eq. 4, the effective contact radius r_c can be obtained. However, for smaller Cl^-–ionosomes of the diameter ≤ ca. 700 nm, the calculated r_c is even smaller than the radii of bare Cl^- ions (181 pm)[25] if the pristine diffusion coefficient of Cl^- (2.03×10^{-9} m^2 s^{-1})[26] in water was employed, which is contrary to the common sense. Let us think carefully about the fusion mechanism of Cl^-–ionosomes with an anodically (water vs. TFT) polarized micro-ITIES. Briefly, after the kiss and fusion of a Cl^-–ionosome with the TFT/water micro-ITIES, the ion-pair dissociation and the accompanying slower diffusion away of BA^+ from the interface towards the bulk of TFT, that is the disassembly of the nanoscale spherical ionic bilayer, is very likely the rate-determining step (RDS). This reasoning is based on the facts that 1) the ionic bilayer of an ionosome is tightly correlated through the nano-spherical ITIES, i.e., the Cl^- monolayer is closely paired with the BA^+ monolayer via the Coulombic attraction, and 2) the radius of BA^+ is far larger than that of Cl^-, and hence upon fusion of an ionosome with the polarized micro-ITIES, BA^+ returns to the bulk of TFT phase slower than that of Cl^- to the aqueous phase. Besides, the solvation structure of the packed Cl^- ions at the aqueous side of a Cl^-–ionosome is expected to be different from the fully solvated Cl^- ions by water molecules in the bulk of water. Therefore, the original diffusion coefficient of Cl^- in water is unreasonable to be used for calculation of r_c. Certainly, the precise value requires a peep into the detailed mechanism of the fusion process and is out of the scope of this study. For a first approximation, we found that employing a 10-fold smaller diffusion coefficient of Cl^- in water for fitting gives a satisfactory contact radius (see Figure 3). Coincidentally, Amatore et al. pointed out that during exocytosis the diffusion coefficient of ions inside a swollen synaptic vesicle should be smaller (about two orders of magnitude) than that in the extracellular fluid.[27] The best-fit parameters for Cl^-–ionosomes with different diameters including k and half-life period ($t_{1/2}$) can be found both in Figure 3 and in Table 1. Note that the parameters of one more best-fitting for a 480 nm Cl^-–ionosome is also listed in Table 1. In general, the contact radius grows as the Cl^-–ionosomes increase in size.

Table 1. Summary of the best-fit *i-t* parameters of Cl^-–ionosomes in different sizes.

diameter / nm	i_p / pA	*mA/V* / s^{-1}[a]	$t_{1/2}$ (exp.) / s[b]	$t_{1/2}$ (calculated) / s[c]	r_c / nm
352	2.18	13.323	0.060	0.055	0.374
480	3.48	14.546	0.050	0.048	1.037
606	4.27	10.828	0.070	0.066	1.554
886	9.59	10.670	0.070	0.065	4.784
1040	12.87	11.213	0.070	0.072	8.305

[a] *mA/V* is analogous to the first-order rate constant, which is obtained by the bulk electrolysis model fitting. [b] $t_{1/2}$ represents the time required for the current to decrease to half of i_p. [c] $t_{1/2}$ (calculated) is calculated by the first-order kinetics equation.

In Figure 4, a total of 101 fusion events were counted during 300 s. Most Cl^-–ionosomes have charges within 800 fC, corresponding to a diameter of 782 nm. Nearly 50% ionosomes have a charge within 100 fC (sized in 278 nm in diameter). Fitting with the Gaussian distribution, Cl^-–ionosomes have charges of 70 ± 24 fC. For a 70 fC Cl^-–ionosome, it contains 4.37×10^5 Cl^-. Most Cl^-–ionosomes are sized in 229 ± 39 nm in diameter, which is consistent with the dynamic light scattering (DLS) measurements shown in Figures S4 and S5 in the SI. The DLS shows an average diameter of 292 nm with a PDI value of 0.005 for Cl^-–ionosomes produced by the chemical polarization (i.e., biphasic distribution of an antagonistic salt, here bis(triphenylphosphoranylidene)ammonium chloride (BACl), under equilibrium) of the water/TFT interface for 72 hours. The monodispersity of Cl^-–ionosomes generated via either electrochemical or chemical polarization (see Figure S5, SI) proves that the Cl^-–ionosomes bearing net charge hardly aggregate and/or coalesce. It provides a platform to observe quantal ion transfer released from the individual polarized nano-spherical ITIES (i.e., ionosome). The average dwell time of the Cl^-–ionosomes is 176 ms, implying a millisecond bulk electrolysis. The relationship between the dwell time and the charge of Cl^-–ionosomes is shown in Figure 4D. It shows that the dwell time and the charge are positively correlated, meaning that larger-sized Cl^-–ionosomes require more time to release Cl^- completely into the water phase. It is interesting that even for large ionosomes, the time to reach the peak current is not very different with the small ones, mostly in the range of 40 to 70 ms.

Effect of Concentration of Aqueous Anions and the Micro-ITIES Area. Keeping the composition of the organic phase (5 mM BATB in TFT) unchanged, the CVs of different aqueous LiCl concentrations (10, 100, and 1000 mM) at the water/TFT micro-ITIES are shown in Figure S6 in the SI. When the aqueous electrolyte concentration (more precisely, activity) is increased by an order of magnitude, theoretically each end of the PPW narrows by 59 mV at room temperature, which obeys the Nernst equation at the ITIES as following:

$$\Delta_o^w \phi = \Delta_o^w \phi_{Cl^-}^\circ - \frac{RT}{F} \ln \frac{\gamma_{Cl^-}^o c_{Cl^-}^o}{\gamma_{Cl^-}^w c_{Cl^-}^w} \qquad (5)$$

where $\Delta_o^w \phi_{Cl^-}^\circ$ is the standard transfer potential of Cl^-, $\gamma_{Cl^-}^w$, $\gamma_{Cl^-}^o$ and $c_{Cl^-}^w$, $c_{Cl^-}^o$ are the activity coefficient and the concentration of Cl^- in the aqueous and the organic phases, respectively. Evolution of the PPW as a function of the aqueous LiCl concentration is fairly in line with the eq. 5 and proves that transfer of Li^+ and Cl^- from water to TFT limits the positive and negative ends of the PPW at the water/TFT micro-ITIES, respectively. Therefore, we changed the Galvani detection potentials with different concentrated LiCl to ensure that the experimental conditions were kept unchanged as much as possible (see Figure 5). With 100 mM LiCl aqueous solution, the collision/fusion signals of the Cl^-–ionosomes disappeared at halfway of the experimental time and is only one-third the collision/fusion number (34 in total) compared to the case of 10 mM LiCl (note that there was no signal when its detection potential was applied again to the identical electrochemical cell). Increasing the LiCl concentration to 1 M, the collision/fusion signals completely disappeared, and a smooth and stable current trace signalling the background charging current was observed throughout the *i–t* detection experiment (Figure 5C). It implies that no any Cl^-–ionosomes are generated in the organic phase via the electrochemical polarization. This phenomenon is contrary to our expectations that Cl^- in higher concentration should form more Cl^-–ionosomes.

However, in effect, higher Cl^- concentration reduces the number of Cl^-–ionosomes. In our previous work, we pointed out that the formation of ionosomes requires the participation of water molecules; and so water not only acts as a solvent but also acts as a reactant.[18a] Note the fact that as the aqueous LiCl concentration increases, the ratio of Li^+ to water molecules also increases significantly, implying a significant decrease in the number of available water molecules per Cl^- upon the nucleation and growth of the Cl^-–ionosomes. It is inferred that compared with the hydrated lithium ions, 1) the first, "inner" hydration layer of chloride ions is looser; 2) the water molecules in the first hydration layer of chloride ions may decrease as the concentration of lithium chloride increases.[28] In brief, Cl^- ions may act as a water sturcture breaker with increasing LiCl concentration to a considerably large value, like 1 M.[29] This causes a significantly ineffective transfer of water molecules via the so-called water finger/chain mechanism[8a] into the TFT phase under an electrical field. The non-supersaturated water at the TFT side cannot trigger the nucleation and further growth into the Cl^-–ionosomes.

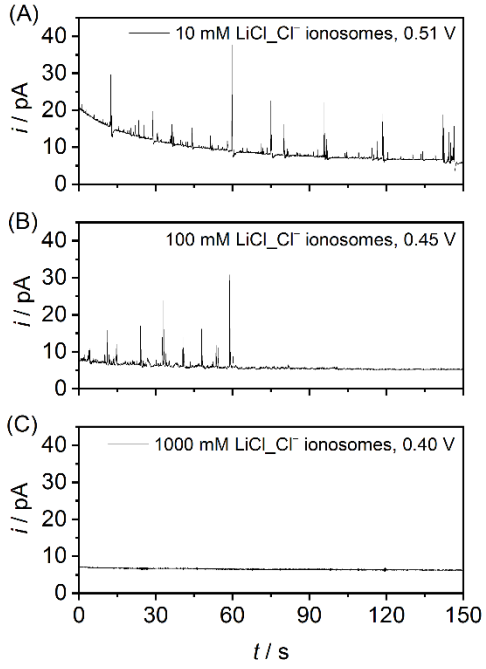

Figure 6. (A, B, and C) Amperometric *i*–*t* curves recorded for collisions and fusions of single Cl^-−ionosomes with a water/TFT ITIES supported at a micropipette (inner diameter: 2.8, 2.6, and 2.9 µm, respectively), in which 10, 100, and 1000 mM LiCl were used as the aqueous electrolytes inside the micropipette for panels A-C. For each panel, 5 mM BATB was employed as the supporting electrolyte in TFT. The other experimental details were found in electrochemical cell 1 in Scheme 1. Note that Figure 5A was reproduced from Figure 2B.

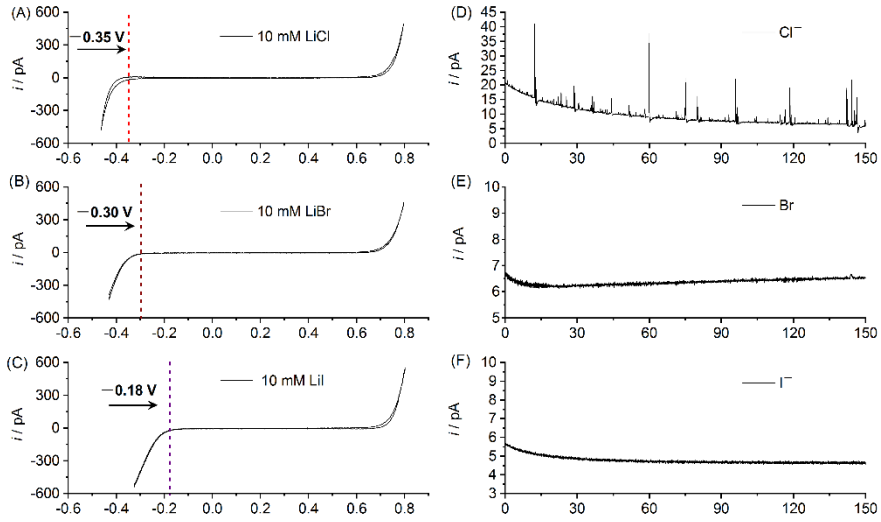

Figure 5. CVs recorded at a micropipette-supported water/TFT ITIES (i.d.: 2.8, 2.4, and 2.5 µm, respectively), where 10 mM (A) LiCl, (B) LiBr, and (C) LiI are the aqueous electrolytes filled inside the micropipette and 5 mM BATB is the supporting electrolyte in the outer TFT phase (see electrochemical cell 2, Scheme 1). Scan rate: 20 mV s^{-1}. (D) The *i*–*t* curve reproduced from Figure 2B. (E) The *i*–*t* curve obtained with 10 mM LiBr as the aqueous phase and a Galvani collecting potential applied at 0.52 V. (F) The *i*–*t* curve obtained with 10 mM LiI as the aqueous electrolyte and 0.58 V as the collecting Galvani potential. It is worth noting that we usually set the detection time for anionic ionosomes to 150 seconds, because most of the ionosomes can be detected within 150 seconds and there are almost no collision/fusion signals in the second 150 seconds. The dashed vertical lines with different colors represent the onset transfer potentials for different anions.

Next, the effect of the water/TFT interfacial area for generation and ensuing in-situ detection of Cl^-−ionosomes was investigated. Detecting Cl^-−ionosomes at a micropipette-supported ITIES with an i.d. of either 250 nm, or 600 nm, and or 2.8 µm is shown in Figure S7 in the SI. When the i.d. of the ITIES is 250 nm, almost no collision/fusion signals are detectable in 150 s. While the collision/fusion events appear sparsely (with a frequency of 79/150 s ≈ 0.53 Hz) when the i.d. of the ITIES is 600 nm. The events are more dense at the ITIES with an i.d. of 2.8 µm (with a frequency of 96/150 s = 0.64 Hz). In brief, larger micro-scaled ITIES facilitates the generation (and also the detection) of ionosomes via the IT reaction. It also explains why the chemical polarizaton in a macroscopic cuvette produces ionosomes readily.

Charge Density of Hydrated Anions. In order to explore the effect from the charge density of hydrated anions on generation and detection of anionic ionosomes, we chose another two aqueous Li^+ electrolytes paired with different anions to replace LiCl in the electrochemical cell 2 (Scheme 1) where the other experimental conditions were kept as unchanged as possible except the Galvani potentials. The charge density of these bare anions varies with the order of $Cl^- > Br^- > I^-$. The CVs are shown in Figure 6, panels A–C, in which the negative ends of the PPW are clearly limited by the transfer of different hydrated anions. Transfer of the common hydrated Li^+ (paired with all anions),

limits the positive end of the PPW. Intuitively, for the transferred anions, the width of PPW reflects their hydrophilicity.[30] It is seen from Figure 6 that the onset transfer potentials are −0.35 V, −0.30 V, and −0.18 V for Cl^-, Br^-, and I^-, respectively. Hence, hydrophilicity of the investigated anions follows the same order as that for the charge density: $Cl^- > Br^- > I^-$. Figure 6E–F shows that the background current trace tends to stabilize after a short time (e.g., within 30 s for panels E and F). Besides, no discrete ionic spikes are observable on the recorded *i–t* curves, as shown in Figure 6E–F. It implies that almost no anionic ionosomes are formed in the organic phase via IT of either Br^- or I^-. The experimental results meet our expectations. The ionosome can be regarded as a nanoscopic spherical ionic capacitor, in which its capacitance is determined by the distance between the hydrated ions and the hydrophobic counterions. Keeping the lipophilic counterion, like BA^+ unchanged, the ease of anionic ionosome formation after the hydrated anion transfer follows the sequence $Cl^- > Br^- > I^-$. And then the interfacial charge (density) is directly proportional to the applied Galvani potential difference.[18a] Thus, polarizing the micro-ITIES strongly with a potentiostat will make the accumulated interfacial charge being too large. Subsequently, the interfacial tension drops significantly obeying the Lippmann electrocapillary equation and the interface emulsifies to increase its interfacial area, which implies that ionosomes are readily to form with a higher charge density of the hydrated ions. The experiments (see Figure 6) conducted with the hydrated anions of varying charge density conform well to the theoretical arguments mentioned above. This phenomenon also confirms that the law of cationic ionosomes is also applicable to anionic ionosomes. In addition, Br^- and $I^-$are chaotropes (i.e., less hydrated than Cl^-) referring to the Hofmeister series.[31] That is, the hydration number of larger anions (than Cl^-) may not meet the necessary (nucleation) conditions for the formation of anionic ionosomes after the break of “water fingers”.[8a, 8d]

The Synergistic Effect between BF_4^- and Cl^-. In our prior work, we discovered that formation of Li^+–ionosomes via electrochemical polarization is enhanced by the addition of a small amount of tetraethylammonium cations (TEA^+) that cross the water/TFT micro-ITIES ahead of Li^+.[18a] This synergistic effect between TEA^+ and Li^+ was justified by the hypothesis that TEA^+ transfer drags some additional water molecules from the aqueous phase into the organic phase. This promotes water supersaturation inside the organic phase, which is beneficial to assembling the Li^+–ionosomes after the Li^+ entry. Similarly, here we chose a typical anion, BF_4^-, that transfer across the ITIES ahead of Cl^- (see Figure S8 in the SI), to study whether they can also enhance the formation of Cl^-–ionosomes. Firstly, with only 10 mM $LiBF_4$ in the aqueous,anionic ionosomes are hardly formed in the absence of Cl^- (not shown). Interestingly, addition of the BF_4^-has a positive effect. With the electrochemical cell 3 (with 10 mM LiCl and 0.5 mM $LiBF_4$ as the aqueous electrolyte filled inside the micropipette, see Scheme 1), the BF_4^- apparently enhances the genenration of Cl^-–ionosomes, resulting in the detected number of the ionosomes increased by 2.7 times (272 in total), as shown in Figure S9, panels B-D, in the SI. Besides, the average size of ionosomes increases from 229 to 290 nm (Figure S10, SI) by virtue of the synergistic effect between BF_4^- and Cl^-. This is in line with our previous observations.[18a] Meanwhile, we also applied the bulk electrolysis model to the *i*–*t* decay analysis in the addition of BF_4^- (Figure S11, SI), and the results show a slight deviation from the ideality for the anionic ionosomes formed in the presence of both BF_4^- and Cl^-. Very likely both BF_4^- and Cl^- contribute to the formation of the negatively charged ionosomes. The increased average size and the nonideality of the *i*–*t* decay behavior support our speculations. Nevertheless, more detailed explanation requires further study of the interactions between the two ions through such as molecular dynamics simulations and state-of-the-art experimental methods.

Conclusion

In summary, we have investigated the properties of anionic ionosomes using a combination of the double-potential step chronoamperometry and a polarized micro-ITIES sensing platform. The characteristics of anionic ionosomes are basically the same as the cationic ones, such as the monodisperse size distribution, its generation affected by ionic charge density and synergistic effect from other easier transferable ions. Besides, we found that fusion of an ionosome with the oppositely charged sensing micro-ITIES follows the bulk electrolysis model. With the advantages

from both the miniaturized ITIES and the collisional electrochemistry, quantitative analysis of the anionic ionosomes one at a time, was achieved successfully. This work is beneficial to investigating the IT reaction in the nano-sized droplets that are dispersed in the immiscible other fluids (which feature even with an extremely low dielectric constant). This work may also be extended to study the pivotal exocytosis mechanism of a synaptic vesicle in both electrophysiology and brain sciences.

Experimental Section

Chemicals. All reagents are analytical grade and used as received without further purification, unlike otherwise mentioned. Lithium chloride (LiCl, 99%) and lithium tetrafluoroborate ($LiBF_4$, 99.99%) were purchased from Aladdin. Lithium iodide (LiI, 99.995%) was obtained from Acros. Lithium bromide (LiBr, 99.9%) and α,α,α-trifluorotoluene (TFT, 99%) were sourced from Alfa Aesar. Bis(triphenylphosphoranylidene)ammonium chloride (BACl) was ordered from Fluka. Lithium tetrakis(pentafluorophenyl)borate diethyl etherate (LiTB) was bought from Boulder Scientific, USA. Bis (triphenylphosphoranylidene)ammonium tetrakis(pentafluorophenyl)borate (BATB) was synthesized as described elsewhere.[32] All aqueous solutions were prepared using the deionized water (≥18.3 MΩ cm) through a Millipore purification system.

Micropipette Fabrication and Characterization. The micropipettes were made from borosilicate glass capillaries (1 mm in outer diameter (o.d.), 0.58 mm in i.d., 10 cm length, with filament) using a laser-based P-2000 pipette puller (Sutter Instrument Co., USA). The parameters for pulling ~3 μm i.d. micropipettes were listed in Table S1 in the SI. Before pulling, all capillaries were cleaned with a fresh piranha solution (Notes: extreme care should be taken when operating with the piranha solution), followed by washing with a copious amount of water and then drying in the oven. The micropipette tip morphology was inspected by either a Mshot ME31 optical microscope (Figure S2A, SI) or a field-emission high-resolution scanning electron microscope (SEM, HITACHI SU8020, Japan) operated at a 15.0 kV accelerating voltage (Figure S2B, SI).

Electrochemical Experiments. Cyclic voltammetry (CV) and chronoamperometry were measured with a CHI model 760E potentiostat (CH Instruments, Shanghai, China) in an undivided two-electrode glass cell that was placed in a grounded Picoamp Booster embedded Faraday cage (CHI200B, CH Instruments, Shanghai, China). The Ag/AgCl wire with the diameter of 0.25 mm was used as the working electrode (WE, placed inside the micropipette) for the aqueous phase, and another one with the diameter of 0.6 mm was used as the counter/reference electrode (CE/RE) placed in the outer organic solution. The scheme of the electrochemical experiments conducted at a micro-ITIES is shown in the left panel of Figure 1.

Electrochemical Experiments. The ionosomes formed spontaneously via a chemical polarization (i.e., biphasic distribution of an antagonistic salt under equilibrium) were sized by the dynamic light scattering (DLS) with a Mastersizer 2000 instrument (Malvern, UK). Chemical polarization was carried out after 72 h from the initial contact between 0.7 mL of 10 mM BACl in water (upper phase) and 2.5 mL of neat TFT (lower phase) in a quartz cuvette (see Figure S4, SI).

Acknowledgements

This work was supported by the National Natural Science Foundation of China (Nos. 21904143, 22108085, 21974032) and the Fundamental Research Funds for the Central Universities, Sun Yat-sen

University, 2021qntd13. This work has also partially emanated from the research of P.P. supported by the European Research Council through a Starting Grant (agreement no. 950038). P.P. also gratefully acknowledges the Academy Research Fellow funding (Grant No. 315739) by the Academy of Finland and the Academy of Finland project funding for PHOTOH2 (Grant No. 334828).

Keywords: single-entity collisional electrochemistry • Cl^-–ionosomes • ITIES • bulk electrolysis

[1] aS. J. Kwon, A. J. Bard, *J. Am. Chem. Soc.* **2012**, *134*, 10777-10779; bE. Dick Jeffrey, T. Hilterbrand Adam, M. Strawsine Lauren, W. Upton Jason, J. Bard Allen, *Proc. Natl. Acad. Sci. U.S.A* **2016**, *113*, 6403-6408; cX. Chang, C. Batchelor-McAuley, R. G. Compton, *Chem. Sci.* **2020**, *11*, 4416-4421.

[2] R. Dasari, D. A. Robinson, K. J. Stevenson, *J. Am. Chem. Soc.* **2013**, *135*, 570-573.

[3] aH. Ma, J. F. Chen, H. F. Wang, P. J. Hu, W. Ma, Y. T. Long, *Nat Commun* **2020**, *11*, 2307; bH. Park, J. H. Park, *Chem. Sci.* **2020**, *11*, 10250-10255.

[4] aT. J. Anderson, B. Zhang, *Acc. Chem. Res.* **2016**, *49*, 2625-2631; bM. Jaugstetter, N. Blanc, M. Kratz, K. Tschulik, *Chem. Soc. Rev.* **2022**, *51*, 2491-2543.

[5] aB.-K. Kim, A. Boika, J. Kim, J. E. Dick, A. J. Bard, *J. Am. Chem. Soc.* **2014**, *136*, 4849-4852; bB.-K. Kim, J. Kim, A. J. Bard, *J. Am. Chem. Soc* **2015**, *137*, 2343-2349; cH. Deng, J. E. Dick, S. Kummer, U. Kragl, S. H. Strauss, A. J. Bard, *Anal. Chem.* **2016**, *88*, 7754-7761.

[6] Z. Guo, S. J. Percival, B. Zhang, *J. Am. Chem. Soc.* **2014**, *136*, 8879-8882.

[7] aX. Huang, H. Deng, C. Liu, J. Jiang, Q. Zeng, L. Wang, *Chem. Eur J.* **2016**, *22*, 9523-9527; bC. Liu, P. Peljo, X. Huang, W. Cheng, L. Wang, H. Deng, *Anal. Chem.* **2017**, *89*, 9284-9291.

[8] aL. Benjamin, *Science* **1993**, *261*, 1558-1560; bR. A. Marcus, *J. Chem. Phys.* **2000**, *113*, 1618-1629; cG. Luo, S. Malkova, J. Yoon, G. Schultz David, B. Lin, M. Meron, I. Benjamin, P. Vanýsek, L. Schlossman Mark, *Science* **2006**, *311*, 216-218; dN. Kikkawa, L. Wang, A. Morita, *J. Am. Chem. Soc.* **2015**, *137*, 8022-8025.

[9] aT. J. Stockmann, Z. Ding, *Anal. Chem.* **2011**, *83*, 7542-7549; bT. J. Stockmann, Y. Lu, J. Zhang, H. H. Girault, Z. Ding, *Chem. Eur. J.* **2011**, *17*, 13206-13216.

[10] J. Guo, Y. Yuan, S. Amemiya, *Anal. Chem.* **2005**, *77*, 5711-5719.

[11] I. Benjamin, *J. Phy. Chem. B* **2013**, *117*, 4325-4331.

[12] M. Shen, R. Ishimatsu, J. Kim, S. Amemiya, *J. Am. Chem. Soc.* **2012**, *134*, 9856-9859.

[13] O. Laforge François, J. Carpino, A. Rotenberg Susan, V. Mirkin Michael, *Natl. Acad. Sci. U.S.A* **2007**, *104*, 11895-11900.

[14] E. Laborda, A. Molina, V. F. Espín, F. Martínez-Ortiz, J. García de la Torre, R. G. Compton, *Angew. Chem., Int. Ed.* **2017**, *56*, 782-785.

[15] A. Doyle Declan, M. Cabral João, A. Pfuetzner Richard, A. Kuo, M. Gulbis Jacqueline, L. Cohen Steven, T. Chait Brian, R. MacKinnon, *Science* **1998**, *280*, 69-77.

[16] aA. Trojánek, V. Mareček, Z. Samec, *Electrochem. Commun.* **2018**, *86*, 113-116; bA. Trojánek, Z. Samec, *Electrochim. Acta* **2019**, *299*, 875-885.

[17] aT. J. Stockmann, L. Angelé, V. Brasiliense, C. Combellas, F. Kanoufi, *Angew. Chem., Int. Ed.* **2017**, *56*, 13493-13497; bT. J. Stockmann, J.-F. Lemineur, H. Liu, C. Cometto, M. Robert, C. Combellas, F. Kanoufi, *Electrochim. Acta* **2019**, *299*, 222-230.

[18] aH. Deng, P. Peljo, X. Huang, E. Smirnov, S. Sarkar, S. Maye, H. H. Girault, D. Mandler, *J. Am. Chem. Soc.* **2021**, *143*, 7671-7680; bL. Huang, J. Zhang, Z. Xiang, D. Wu, X. Huang, X. Huang, Z. Liang, Z.-Y. Tang, H. Deng, *Anal. Chem.* **2021**, *93*, 9495-9504.

[19] M. M. Vieira, J.-F. Lemineur, J. Médard, C. Combellas, F. Kanoufi, J.-M. Noël, *J. Phys. Chem. Lett.* **2022**, *13*, 5468-5473.

[20] T. Kakiuchi, *Electrochem. Commun.* **2000**, *2*, 317-321.

[21] E. Laborda, A. Molina, *Curr. Opin. Electrochem.* **2021**, *26*, 100664.

[22] E. R. Nightingale, *J. Phys. Chem.* **1959**, *63*, 1381-1387.

[23] A. J. Bard, L. R. Faulkner, *Electrochemical Methods: Fundamentals and Applications*, 2nd ed., John Wiley & Sons, New York, **2002**, pp, 424-425.

[24] A. Trojánek, V. Mareček, Z. Samec, *Electrochim. Acta* **2020**, *354*, 136653.

[25] R. D. Shannon, C. T. Prewitt, *Acta Crystallogr. B. Struct. Sci. Cryst. Eng. Mater.* **1969**, *25*, 925-946.

[26] P. Atkins, J. D. Paula, J. Keeler, *Atkins' Physical Chemistry,* 11th ed. Oxford University Press, Oxford, **2018**, pp, 704.

[27] C. Amatore, Y. Bouret, L. Midrier, *Chem. Eur. J.* **1999**, 5, 2151-2162.

[28] R. H. Tromp, G. W. Neilson, A. K. Soper, *J. Chem. Phys*. **1992**, *96*, 8460-8469.

[29] I. Harsányi, L. Pusztai, *J. Chem. Phys.* **2005**, 122, 124512.

[30] aT. Kakiuchi, *Anal. Chem.* **2007**, *79*, 6442-6449; bT. J. Stockmann, Z. Ding, J. *Electroanal. Chem*. **2010**, *649*, 23-31.

[31] D. Bastos-González, L. Pérez-Fuentes, C. Drummond, J. Faraudo, *Curr. Opi. Colloid Interface Sci.* **2016**, *23*, 19-28.

[32] J. Fermín, D.; Dung Duong, H.; Ding, Z.; Brevet, o.; H. Girault, H. *Phys. Chem. Chem. Phys.* **1999**, *1*, 1461-1467.

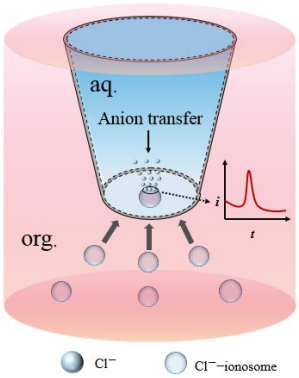

With single-entity collisional electrochemistry, anionic ionosomes (i.e., negatively-charged nanoscopic water clusters wrapped by by an ionic bilayer) are quantitatively analysed at a positively polarized micro-water/oil interface. When Cl^-–ionosomes in the organic phase collide/fuse with the polarized interface formed at the very tip of a micropipette, chloride ions will be released from an ionosome into the water phase manifested as a current spike along the timeline. Fusion mechanism along with sizing of ionosomes are readily uncovered via detailed analysis of the current spikes.